CRYSTAL GROWTH & DESIGN

Article

pubs.acs.org/crystal

Tuning the Morphological, Optical, and Antimicrobial Properties of α-Ag_2WO_4 Microcrystals Using Different Solvents

Camila C. de Foggi,*[,†] Regiane C. de Oliveira,[‡] Maria T. Fabbro,[‡] Carlos E. Vergani,[†] Juan Andres,[§] Elson Longo,[∥] and Ana L. Machado[†]

[†]Department of Dental Materials and Prosthodontics, School of Dentistry at Araraquara, São Paulo State University (UNESP), Araraquara, Brazil

[‡]Chemistry Institute at São Carlos, São Carlos Federal University (UFSCar), São Carlos, Brazil

[§]University Jaume I, Castellón, Spain

[∥]Chemistry Institute at Araraquara, São Paulo State University (UNESP), Araraquara, Brazil

ABSTRACT: New, effective antimicrobial agents are constantly being evaluated for addressing the increased prevalence of bacterial and fungal infections and emerging drug resistance. In this study, α-Ag_2WO_4 microcrystals were prepared by controlled coprecipitation (90 °C for 10 min) in different solvents (e.g., water, an alcoholic solution, and an ammoniacal solution). From the X-ray diffraction results, the newly synthesized α-Ag_2WO_4 microcrystals are well-indexed to the orthorhombic structure. Two morphologies were seen by field-emission scanning electron microscopy: microrods in the alcoholic solution and flowerlike structures in water and the ammoniacal solution. The synthesized α-Ag_2WO_4 microcrystals exhibited antimicrobial activity against *Candida albicans*, *Escherichia coli*, and methicillin-resistant *Staphylococcus aureus*. In addition, the antibacterial performance of the α-Ag_2WO_4 samples as a function of their structural and morphological features was discussed.

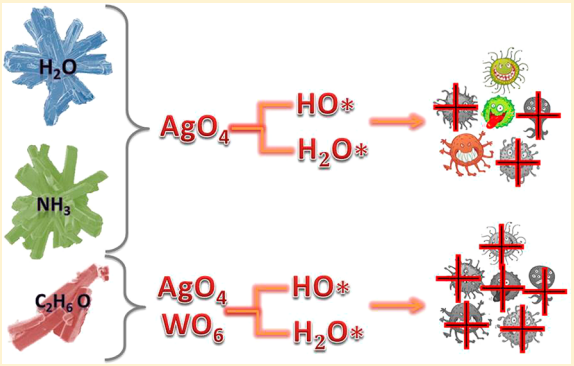

1. INTRODUCTION

Transition-metal tungstates, which represent an important class of functional materials, have been intensely investigated because of their interesting structures; intriguing physicochemical properties; and diverse applications as photoluminescence agents, photocatalysts, sensors, and antimicrobial and anticancer materials.[1−9] Among the family of tungstates, silver tungstate, particularly α-Ag_2WO_4, exhibits interesting physical and chemical properties that can be modulated for various applications, including sensors, optical devices, photodegradation, and catalytic processes.[10−29] Notably, α-Ag_2WO_4 is interesting because of its electronic structure, which is related to the combination of covalent, ionic, and metallic chemical bonds. Different studies have demonstrated that α-Ag_2WO_4 exhibits good photocatalytic activity under visible light for the degradation of organic dyes and for the destruction of *Escherichia coli* (*E. coli*).[30,31]

Recently, research has been focused on the preparation of antimicrobial materials for multiple applications, such as sanitary materials and household, food packaging, medical, and military items.[32−38] In this context, and in view of the critical need to discover families of new materials, our group carried out a study using α-Ag_2WO_4 as the antibacterial agent[12,39] and β-Ag_2MoO_4 as the antifungal agent.[40] However, the resulting activities are extremely sensitive to experimental conditions, e.g., the solvent used during the synthesis, leading to potentially different behavior and performance. Herein, the application of α-Ag_2WO_4 as an antimicrobial agent was discussed; to this end, α-Ag_2WO_4 samples were synthesized by controlled coprecipitation (CP) and characterized using three separate solvents: water, alcoholic solution, and ammoniacal solution. The sample structures were examined by X-ray diffraction (XRD) and Raman spectroscopy, while the crystal morphology was observed by field-emission scanning electron microscopy (FE-SEM). Ultraviolet−visible (UV−vis) diffuse reflectance spectroscopy and photoluminescence (PL) measurements were used to analyze the optical properties. The antimicrobial activity against planktonic cells, i.e., fungi *Candida albicans* (*C. albicans*), Gram-positive methicillin-resistant *Staphylococcus aureus* (MRSA), and Gram-negative *E. coli*, was evaluated by determining the minimum inhibitory concentration (MIC) and minimum fungicidal or bactericidal concentration (MFC/MBC). The remaining paper is divided into three sections. The experimental details are discussed in section 2, including experimental techniques and antimicrobial activities of the different as-synthesized α-Ag_2WO_4 micro-

Received: June 6, 2017
Revised: November 9, 2017
Published: November 13, 2017

DOI: 10.1021/acs.cgd.7b00786
Cryst. Growth Des. 2017, 17, 6239−6246

crystals, followed by the results and discussion in sections 3 and 4, respectively.

2. MATERIALS AND METHODS

2.1. Synthesis of α-Ag_2WO_4 Using Different Solvents. The α-Ag_2WO_4 microcrystals were synthesized by CP using water, an alcoholic solution, and an ammoniacal solution as the solvents, without the use of surfactants. Sodium tungstate dihydrate ($Na_2WO_4{\cdot}2H_2O$; 99.5% purity, Synth) and silver nitrate ($AgNO_3$; 99.8% purity, Sigma-Aldrich) were used as the starting precursors. With the use of water as the solvent, the two precursors ($Na_2WO_4{\cdot}2H_2O$, 1 mmol; $AgNO_3$, 2 mmol) were separately dissolved in two beakers, each containing 50 mL of deionized water, affording solutions 1 and 2, respectively. Next, solution 2 was added in a dropwise manner into solution 1 under vigorous magnetic stirring at 90 °C for 10 min.

During the synthesis using the alcoholic solution as the solvent, two solutions (1 and 2) were also separately prepared. First, $Na_2WO_4{\cdot}2H_2O$ (1 mmol) was dissolved in 50 mL of an alcoholic solution (50% anhydrous ethanol, 99.95% purity, Synth, and 50% water) and $AgNO_3$ (2 mmol) was dissolved in 50 mL of water. Next, solution 2 was added to solution 1 in a dropwise manner with vigorous stirring at 90 °C for 10 min.

Using the ammoniacal solution as the solvent, solution 1 was prepared by the dissolution of $Na_2WO_4{\cdot}2H_2O$ (1 mmol) in 50 mL of deionized water, and ammonium hydroxide solution (34%, Sigma-Aldrich) was added until a pH of 11 was reached. Separately, solution 2 was obtained by dissolving $AgNO_3$ (2 mmol) in 50 mL of deionized water. Solution 2 was then added in a dropwise manner to solution 1 under vigorous magnetic stirring, and the mixture was heated at 90 °C for 10 min.

The precipitates were collected by centrifugation and washed several times with water until a pH of 7 was attained. Then, the powders were dried at 60 °C for 12 h.

2.2. Sample Characterization. The α-Ag_2WO_4 microcrystal structure was examined by XRD using a Rigaku-DMax/2500PC (Japan) diffractometer, with Cu Kα radiation (λ = 1.5406 Å), in the 2θ range of 10°−70° at a scanning rate of 2°/min. Raman spectra were recorded using a T64000 spectrometer (Horiba Jobin-Yvon, Japan) coupled to a CCD Synapse detector and an argon-ion laser, operating at 514 nm with a maximum power of 7 mW. The spectra were measured in the 280−950 cm^{-1} range. UV−vis spectra were recorded on a Varian spectrophotometer (model Cary 5G, United States) in the diffuse-reflection mode. The sample morphologies were examined by FE-SEM (Supra 35-VP Carl Zeiss, Germany) operated at 15 kV. PL measurements were carried out using a Monospec 27 monochromator (Thermo Jarrell Ash, United States) coupled with an R955 photomultiplier (Hamamatsu Photonics, Japan). A krypton-ion laser (Coherent Innova 200 K, United States; λ = 350 nm) was used as the excitation source with an incident power of approximately 14 mW on the sample. All measurements were carried out at room temperature.

2.3. Antimicrobial Effects of α-Ag_2WO_4 Microcrystals Obtained in Different Solvents. In this study, the antimicrobial activity of the synthesized α-Ag_2WO_4 microcrystals was investigated against one yeast, *C. albicans*, one Gram-positive bacterium, MRSA, and one Gram-negative bacterium, *E. coli*. The antimicrobial activity of the α-Ag_2WO_4 microcrystals was evaluated by the measurement of the MICs and MFCs/MBCs for planktonic cells of the three strains from the American Type Culture Collection (ATCC): *C. albicans* ATCC 90028, *E. coli* ATCC 8739, and MRSA ATCC 33591. Susceptibility tests were performed using the Clinical and Laboratory Standards Institute broth microdilution method [documents M27-A3 (2008) and M7-A7 (2006) for yeast and bacteria, respectively].[41,42]

Candida albicans were cultured according to the methodology described by Fabbro et al.[40] Briefly, the strain were cultured from frozen stock onto Sabouraud dextrose agar plus chloramphenicol (0.05 g/L, SDA, Acumedia Manufacturers Inc., Baltimore, MD) and incubated for 48 h at 37 °C before being tested. MRSA and *E. coli* were cultured onto Mueller−Hinton agar plates (Acumedia Manufacturers Inc., Baltimore, MD) and incubated at 37 °C for 24−48 h. A loopful of fresh cells of each microorganism grown on the agar plates was transferred to an RPMI-1640 culture medium (Sigma-Aldrich, St. Louis, MO) for *C. albicans*; tryptic soy broth (TSB, Acumedia Manufacturers, Inc. Baltimore, MD) for MRSA; and Mueller−Hinton broth (MHB, Acumedia Manufacturers, Inc. Baltimore, MD) for *E. coli*. After overnight incubation at 37 °C in an orbital shaker (75 rpm), the cells were harvested and washed twice using a phosphate-buffered saline (PBS, pH 7.2) solution at 5 000*g* for 5 min. *C. albicans* cells were resuspended in the medium RPMI-1640, and bacterial cells were resuspended in TSB and MHB culture media for MRSA and *E. coli*, respectively. *C. albicans*, MRSA, and *E. coli* suspensions were spectrophotometrically standardized to a final concentration of 10^7 colony-forming units per milliliter (CFU/mL).

The MICs and MFCs/MBCs were determined by incubating the microorganisms for 24 h at 37 °C on 96-well microtiter plates, exposed to serial dilutions of each α-Ag_2WO_4 solutions (from 1000 to 0.061 μg/mL) in specific culture media. Positive controls were inoculated with microbial suspension but no α-Ag_2WO_4 microcrystals, while the negative controls consisted of uninoculated culture medium. MICs were recorded as the lowest concentrations of each solution to achieve complete inhibition of growth (without visible growth by visual inspection).[43,44]

MFCs/MBCs were determined by inoculating 25 μL aliquots, taken from 10-fold serial dilutions (10^{-1} to 10^{-8}) of each well, on plates containing SDA for *C. albicans* and Mueller−Hinton agar for MRSA and *E. coli*, in duplicate. After the cells were incubated at 37 °C for 24−48 h, the CFU/mL was calculated and $\log_{10}$-transformed. The MFCs/MBCs were defined as the lowest concentrations of each of the α-Ag_2WO_4 solutions that result in no microbial growth on plates.[43,44] The assays were performed in three independent experiments, in triplicate.

3. RESULTS

3.1. X-ray Diffraction. Figure 1 displays the XRD patterns of the α-Ag_2WO_4 obtained employing water and the alcoholic

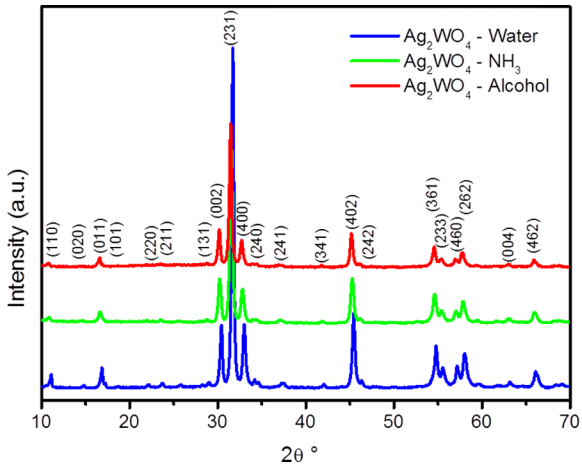

Figure 1. XRD patterns of the α-Ag_2WO_4 microcrystals synthesized in water, ammoniacal (NH_3), and alcoholic solutions.

and ammoniacal solutions. All of the diffraction peaks observed for the α-Ag_2WO_4 are related to the orthorhombic structure with the *Pn2n* space group (C_{2v}^{10} symmetry). This result is in concordance with the Joint Committee on Inorganic Crystal Structure Database card no. 4165[20,45] without secondary phases.

3.2. Raman Spectroscopy. Raman spectroscopy is a powerful and effective measurement for investigating the short-range ordered structure (Figure 2). Twelve active modes are observed in the Raman spectra of α-Ag_2WO_4 samples obtained

DOI: 10.1021/acs.cgd.7b00786
Cryst. Growth Des. 2017, 17, 6239−6246

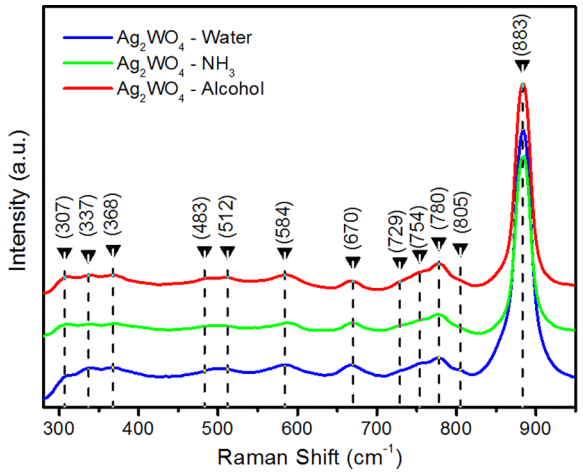

Figure 2. Raman spectra of the α-Ag_2WO_4 microcrystals synthesized in water, ammoniacal (NH_3), and alcoholic solution.

using different solvents. The most intense peak at 883 cm^{-1} corresponds to the symmetric stretching of the O–W–O bonds in the $[WO_6]$[25] and the bending modes of the Ag–O–W unit.[20,46] The active modes between 805 and 483 cm^{-1} correspond to the vibration in the $[WO_6]$ clusters, while those observed between 368 and 307 cm^{-1} correspond to the vibrational modes of $[AgO_x]$ (x = 7, 6, 4, and 2) clusters.[47]

3.3. FE-SEM Analysis. Figure 3 presents the FE-SEM micrographs for the α-Ag_2WO_4 synthesized in water and in the ammoniacal and alcoholic solutions.

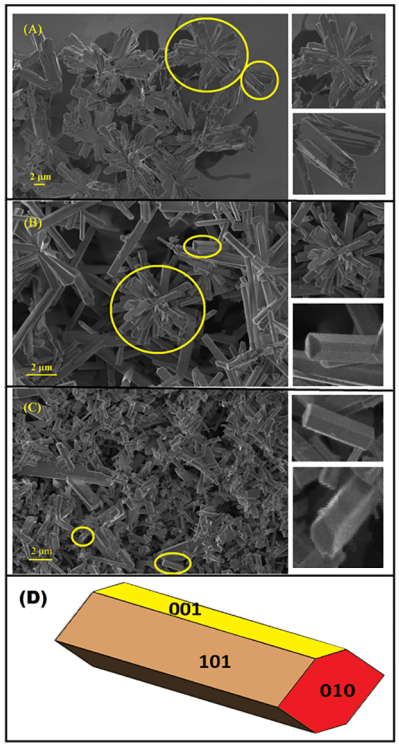

Figure 3. Micrographs of the α-Ag_2WO_4 microcrystals synthesized in water (A), ammoniacal solution (NH_3) (B), and alcoholic solution (C). Illustrative scheme for the α-Ag_2WO_4 crystal with the crystallographic planes (001), (101), and (010) for the three faces (D).

A considerable amount of three-dimensional (3D) flowerlike α-Ag_2WO_4 microcrystals are observed in the aqueous solution. Clearly, these structures are essentially composed of aggregated nanorod particles exhibiting partial orientation and attachment on the irregular faces (Figure 3A). These crystals exhibit an agglomerate nature but are observed as hexagonal rods, which are grown in the y-axis along the [010] direction. Several nanocrystallites exhibit nucleation and grow into small nanorods. To reduce the system energy, these small nanorods have a tendency to clump together, affording 3D flowerlike α-Ag_2WO_4. The same 3D flowerlike α-Ag_2WO_4 structures are obtained using the ammoniacal solution (Figure 3B). However, in this case, the crystals exhibit three faces, with the (001), (101), and (010) crystallographic planes, which are more defined than the crystals obtained using water as solvent. Figure 3D shows these faces of the α-Ag_2WO_4 and the index of the crystal planes on the rod that was previously done by Roca et al.[39] by means of modeling. With the synthesis using the alcoholic solution, α-Ag_2WO_4 nanorods with three faces are observed, and the same crystallographic planes as those observed in the case of the α-Ag_2WO_4 structures synthesized using the ammoniacal solution (Figure 3C) are seen.

3.4. UV–Vis Absorption Spectroscopy. The optical bandgap energy (E_{gap}) was estimated using the method proposed by Kubelka and Munk,[48] which can be summarized by eq 1:

$$[F(R_\infty)h\nu] = C_1(h\nu - E_{gap})^n \quad (1)$$

Here, $F(R_\infty)$ is the Kubelka–Munk function; R_∞ is the reflectance; $h\nu$ is the photon energy; C_1 is a proportionality constant; E_{gap} is the optical band gap; and n is a constant associated with different electronic transitions (n = 0.5, 2, 1.5, and 3 for directly allowed, indirectly allowed, directly forbidden, and indirectly forbidden transitions, respectively).

The optical absorption spectra for the α-Ag_2WO_4 are subject to direct electronic transitions.[18,49] Therefore, after obtaining the $F(R_\infty)$ value from the Kubelka–Munk equation and plotting a graph of $[F(R_\infty)h\nu]^2$ as a function of $h\nu$, the E_{gap} values for α-Ag_2WO_4 were estimated by extrapolating the linear portion of the UV–vis curves. Figure 4 shows the UV–vis diffuse reflectance spectra and E_{gap} values of the α-Ag_2WO_4 microcrystals synthesized in water and in the alcoholic and ammoniacal solutions.

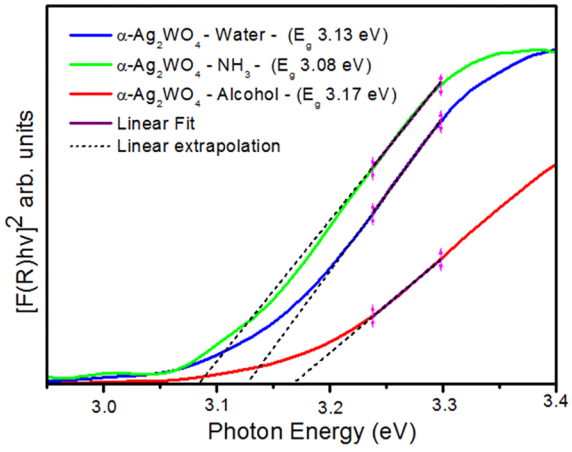

Figure 4. UV–vis diffuse reflectance of the α-Ag_2WO_4 microcrystals synthesized in water, ammoniacal (NH_3), and alcoholic solutions.

DOI: 10.1021/acs.cgd.7b00786
Cryst. Growth Des. 2017, 17, 6239–6246

3.5. Photoluminescence. Figure 5a displays the room-temperature PL spectra of the three samples of α-Ag_2WO_4 microcrystals synthesized in water and in the alcoholic and ammoniacal solutions at an excitation wavelength of 350 nm. The PL bands of α-Ag_2WO_4 correspond to the recombination between electron−hole pair processes and the electronic transition among the valence band (mainly formed by 2p levels of O atoms and 4d levels of Ag atoms) and the conduction band (mainly composed by 5d levels of W atoms). The spectra exhibit typical broad band profiles as a result of multiple relaxation pathways, including the contribution of many energy states inside the band gap. This behavior, which is associated with the structural mess of α-Ag_2WO_4, endorses the existence of extra electronic levels in the forbidden band gap of the semiconductor.[50]

To enhance understanding of the PL properties and their relation to the structural order−disorder of the lattice, the PL curves were deconvoluted with the PeakFit program[51] (Figure 5a). The curve was simulated through the overlapping peaks, and the separate influence of each component was evaluated by their corresponding areas and intensities. Hence, PL profiles are arranged by the addition of three peaks by using the area Voigt function for the α-Ag_2WO_4 synthesized in the alcoholic and ammoniacal solutions, and four peaks were used for the α-Ag_2WO_4 microcrystals synthesized in water. The peak positions were fixed in a position of the spectrum. These four peaks match to blue (447 nm), green (510 nm), orange (613 nm), and red (750 nm) and agree with the position at which the maxima of the curve are observed. Figure 5b shows the percentage contribution for each area.

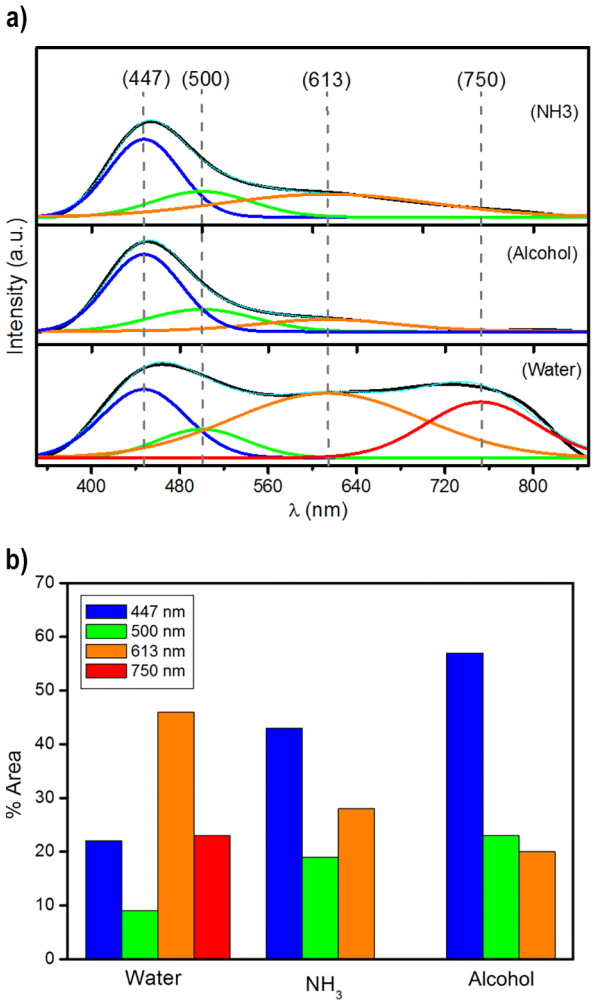

Figure 5. (a) PL spectra and deconvolution PeakFit of PL spectra of the α-Ag_2WO_4 microcrystals synthesized in water, ammoniacal (NH_3), and alcoholic solution. (b) Percentage of area obtained via PL spectra deconvolution of the α-Ag_2WO_4 microcrystals synthesized in water, ammoniacal (NH_3), and alcoholic solution.

3.6. Antimicrobial Effects of the α-Ag_2WO_4 Microcrystals Synthesized Using Different Solvents. The results showed that all the obtained microcrystals exhibit fungistatic and fungicidal activity against *C. albicans*. Moreover, for each of the three samples obtained, namely, α-Ag_2WO_4 synthesized in water and in the alcoholic and ammoniacal solvents, the concentration that completely inhibits visible growth by visual inspection (i.e., the MIC value) also does not allow the growth of colonies in the agar plates (MFC). However, using the alcoholic solution as the solvent, a lower MIC/MFC value (3.90 μg/mL) compared to those observed for the samples synthesized using water (7.81 μg/mL) and the ammoniacal solution (7.81 μg/mL) is observed (Figure 6). Notably, even at concentrations less than the MIC/MFC, the α-Ag_2WO_4 microcrystals can reduce yeast growth. With the incubation of *C. albicans* in the absence of α-Ag_2WO_4 microcrystals, a count of 6.1 $\log_{10}$ CFU/mL is obtained (control). At sub-MIC/MFC concentration (1.95 μg/mL), the sample synthesized using the alcoholic solution reduces *C. albicans* growth by greater than 4 orders of magnitude (to approximately 2.0 $\log_{10}$ CFU/mL, Figure 6). At 0.98 and 0.49 μg/mL, the counts of *C. albicans* are also less than that of the control (3.5 $\log_{10}$ CFU/mL and 4.5 $\log_{10}$ CFU/mL, respectively). Although the effects of the α-Ag_2WO_4 microcrystals synthesized using water and the ammoniacal solution are less pronounced, at 3.90 μg/mL (half of the MIC/MFC), the yeast growth is reduced to approximately 2.4 $\log_{10}$ CFU/mL and 3.1 $\log_{10}$ CFU/mL, respectively. Compared with the control, the reduction of approximately two logs is also observed at 1.95 μg/mL and

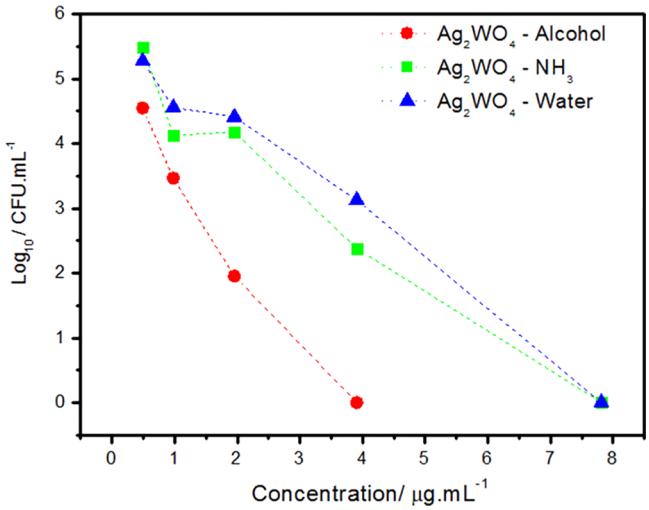

Figure 6. Summary of $\log_{10}$ CFU/mL values of *C. albicans* obtained for the subinhibitory concentrations of the α-Ag_2WO_4 synthesized in water, ammoniacal (NH_3) and alcoholic solution. Control = 6.6 $\log_{10}$ CFU/mL.

DOI: 10.1021/acs.cgd.7b00786
Cryst. Growth Des. 2017, 17, 6239−6246

0.98 μg/mL for water (to ~4.2 $\log_{10}$ CFU/mL) and the ammoniacal solution (to ~4.4 $\log_{10}$ CFU/mL), respectively.

The results obtained from the microbiological tests performed with MRSA revealed that for the three solvents used to synthesize α-Ag_2WO_4 microcrystals, the MIC values were the same as the MBCs. When the microcrystals were synthesized using the alcoholic solution, the MIC/MBC (15.62 μg/mL) is less than that observed for the microcrystals synthesized using the ammoniacal solution (62.5 μg/mL), and the bactericidal activities of both α-Ag_2WO_4 microcrystals are greater than that observed for the samples obtained using water (125 μg/mL). In addition, Figure 7 shows that compared with

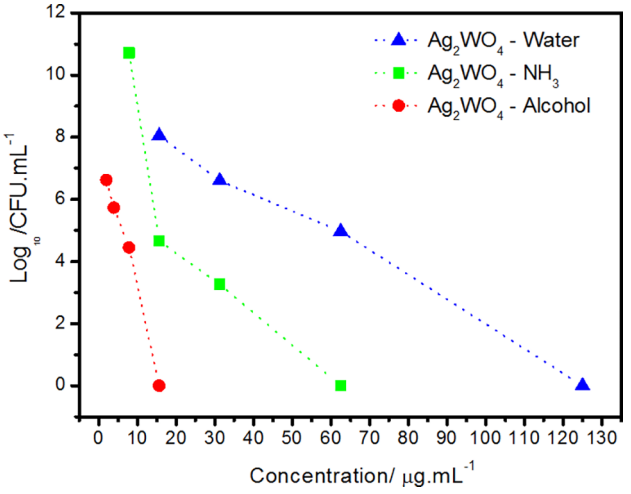

Figure 7. Summary of $\log_{10}$ CFU\mL values of MRSA obtained for the subinhibitory concentrations of the α-Ag_2WO_4 microcrystals synthesized in water, ammoniacal (NH_3) and alcoholic solution. Control = 8.6 $\log_{10}$ CFU\mL.

the control (8.6 $\log_{10}$ CFU/mL), at half of the MIC/MBC, bacterial growth is reduced by approximately four logs for the α-Ag_2WO_4 microcrystals synthesized using the alcoholic solution (to 4.4 $\log_{10}$ CFU/mL), five logs for the microcrystals synthesized using the ammoniacal solution (to 3.2 $\log_{10}$ CFU/mL), and three logs using water (to 4.9 $\log_{10}$ CFU/mL).

Figure 8 shows the $\log_{10}$ CFU/mL values of *E. coli* when incubated with subinhibitory concentrations of the evaluated α-Ag_2WO_4 microcrystals. For the three samples synthesized in the different solvents, the MIC and MBC values were coincident. In addition, the same MIC/MBC (0.49 μg/mL) is observed for the microcrystals synthesized using the alcoholic and ammoniacal solutions. This value is less than that observed using water (MIC/MBC = 0.97 μg/mL). The incubation of the bacteria in the presence of one-half the MIC of the microcrystals led to the reduction in bacterial growth, relative to the control (7.2 $\log_{10}$ CFU/mL), of approximately four logs for the α-Ag_2WO_4 microcrystals synthesized using the alcoholic solution and water (~3.4 $\log_{10}$ CFU/mL for both samples) and three logs for those synthesized in the ammoniacal solution (~4.3 $\log_{10}$ CFU/mL). Notably, the concentrations required to inactivate and kill *E. coli* are considerably less than those needed to achieve the same antimicrobial effects on *C. albicans* and MRSA planktonic cells.

4. DISCUSSION

In this study, α-Ag_2WO4 microcrystals were successfully synthesized by CP using three separate solvents: water,

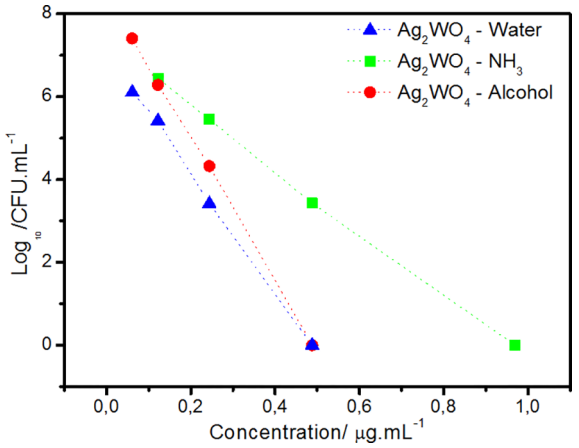

Figure 8. Summary of $\log_{10}$ CFU\mL values of *E. coli* obtained for the subinhibitory concentrations of the α-Ag_2WO_4 microcrystals synthesized in water, ammoniacal (NH_3), and alcoholic solution. Control = 7.2 $\log_{10}$ CFU\mL.

alcoholic solution, and ammoniacal solution. The CP method of synthesis, generally, produces ceramic materials with structural defects, such as distortions in the chemical bonds, vacancies, and surface/interfaces defects, which diminish the symmetry of the structure. Local distortions are defects at short-range, as is evidenced by the distances of the silver−oxygen bond (Ag−O) and tungsten−oxygen bond (W−O). Distortions (defects) in these chemical bonds decrease symmetry at short-range.

The relative intensities and sharp diffraction peaks of the XRD patterns (Figure 1) indicated that the obtained microcrystals are well-crystallized. However, a small widening of the peaks can be observed, suggesting a little disorder at long range in the structure. The intensity and width of the peaks in the Raman spectra also reflect these distortions at short range. Besides that, the Raman peaks (Figure 2) clearly indicated that the α-Ag_2WO_4 structure is similar to that reported previously in the literature.[20,25,46,47]

FE-SEM images are essential for the study of the morphological evolution of α-Ag_2WO_4 synthesized using different solvents. Gong et al.[52] and Chen et al.[53] have independently explained that obtaining nanorod morphologies is related to the oriented aggregation mechanism, involving the natural self-organization of neighbor particles beside a mutual crystallographic orientation. The α-Ag_2WO_4 crystals obtained using the three solvents exhibit distinguished morphologies. When the reaction occurs in water and ammoniacal solution, the reactants are dispersed more regularly than in the alcoholic solution, and the growth of the crystal nucleus is subordinated to less confinement in a boiling droplet of the medium. Consequently, α-Ag_2WO_4 is predisposed to form a flowerlike morphology in water and the ammoniacal solution (Figure 3A,B), but it forms nanorods when using the alcoholic solution as the solvent (Figure 3C).

The results show that the flowerlike morphology of α-Ag_2WO_4 obtained using water has a more defective surface than that observed using ammoniacal solution as the solvent. This is because of a higher reaction rate in pure water that results in a fast and messy growth. In the presence of ammonium, the diammine complex $[Ag(NH_3)_2]^+(aq)$ is formed that makes difficult the release of Ag cations along the α-Ag_2WO_4

DOI: 10.1021/acs.cgd.7b00786
Cryst. Growth Des. 2017, 17, 6239−6246

formation process, thereby forming flowers with a more defined surface.

From the UV−vis spectra, the E_{gap} values of the α-Ag_2WO_4 microcrystals were estimated. The E_{gap} values are 3.13, 3.08, and 3.17 eV for the α-Ag_2WO_4 microcrystals synthesized using water, the ammoniacal solution, and the alcoholic solution, respectively. Significant changes are not observed in the E_{gap} values of the Ag_2WO_4 microcrystals.

PL measurements were performed in order to study the optical properties of materials. As the absorption edge of the α-Ag_2WO_4 microcrystals synthesized in different solvents is approximately 3.10 eV (400 nm) (Figure 4), according to the hypothesis of Longo et al.[54] the PL process on the oxide semiconductor does not correspond to a band-to-band process.

α-Ag_2WO_4 is composed of $[WO_6]$ and $[AgO_x]$ (x = 2, 4, 6, and 7) clusters in a crystal lattice.[55] In addition, this orthorhombic structure can be thought of in terms of a network of $[WO_6]$ and $[AgO_x]$ clusters, connected by strong bonds ($[\cdots[WO_6]-[AgO_x]-[WO_6]\cdots]$) between themselves.[56,57] Therefore, herein, the bonds between the $[WO_6]$ and $[AgO_x]$ clusters in the structure are presumably dissimilar because of the distortion in the $[WO_6]$ complex clusters, promoting a slight deformation in the Ag−O and W−O bonds. Moreover, these distortions can induce the symmetry break in the lattice, leading to the formation of novel intermediate levels within the band gap and charge gradients among the clusters, resulting in the polarization and formation of the $[WO_6]'/[WO_6]^{\bullet}$ or $[AgO_x]'/[AgO_x]^{\bullet}$ clusters.

According to our wide-band model, the distorted $[WO_6]$ octahedral clusters, which are classified as shallow defects, generate emissions in the blue-light region; their corresponding peaks are observed at 447 and 500 nm. The peaks at 613 and 750 nm, corresponding to the emissions in the red-light region, are related to the $[AgO_x]$ clusters with Ag or O vacancies[25] (Figure 5b). Using the alcoholic solution as the solvent, distortions in the $[WO_4]$ clusters are more pronounced as the contribution of more energetic levels is evidenced by blue and green component areas. Using the ammoniacal solution as the solvent, the blue component decreases due the reduction in the energetic defects and the intensification in the contribution of deep defects related with electronic transitions in the red regions, corresponding to the increase in the amount of tetrahedral $[AgO_x]$ distorted clusters (Figure 5b). For the α-Ag_2WO_4 microcrystals synthesized in water, the maximum absorption in the orange region (peak at 613) becomes more pronounced, and a new component in the red-light region is observed, with the increasing contribution of deep defects (Figure 5b). Consequently, in comparison to the other solvents, water promotes more distortion in the tetrahedral $[AgO_x]$ clusters, related to the less energetic defects. Considerable differences in the PL profiles of the α-Ag_2WO_4 crystals can be explained by differences in the surface defects caused by the solvents, which affect the attachment (agglomeration), crystal formation, and growth processes as a result of the dynamics of particle−particle collisions. However, additional issues may too be implicated, including the degree of aggregation; the orientation among particles; and the variation in the morphology, particle size distribution, and surface defects (Figure 3A−C). All of these factors affect the PL emission.

The ability of α-Ag_2WO_4 to generate electron−hole pairs is related to the intrinsic defects, in the form of distortions or vacancies, on $[WO_6]$ (shallow defects).[39] The $[WO_6]$ distorted clusters, with O atom vacancies ($[WO_6]^{\bullet}$), are known to interact with H_2O, affording ·OH* and ·$H^{\bullet}$. On the other hand, the $[WO_6]$ distorted clusters with e′ excess ($[WO_6]'$) react with O_2 and generate O_2'. Then, the newly formed O_2' and $H^{\bullet}$ react to form O_2H^*[39,40,44,58] (Figure 9).

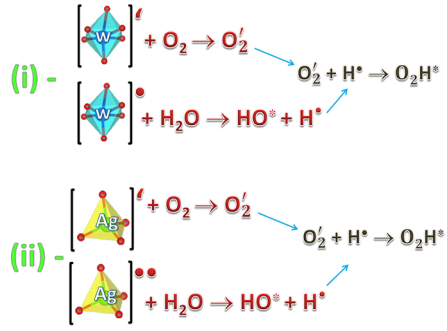

Figure 9. Proposed reaction mechanism for the generation of the oxidative radicals by the catalysts α-Ag_2WO_4 microcrystals.

According to previous studies, these oxidizing radicals, OH* and O_2H^*, are mainly responsible for bacterial death. These radicals are toxic to bacteria and can oxidize organic compounds of the cells, causing breakdown of the cell membranes and damage to protein structure and the intracellular system, thus resulting in the death of the microorganisms.[58−62]

For the α-Ag_2WO_4 microcrystals synthesized using the ammoniacal solution and water, the maximum absorption is in the red region of the spectrum, as observed by PL spectra and deconvolution (Figure 5a,b); hence, they contain only distorted $[AgO_x]$ clusters (modifier network), which are available to produce a small amount of OH* and ·O_2H^*. On the other hand, the α-Ag_2WO_4 synthesized using the alcoholic solution exhibits the highest amount of defects in the blue and red regions of the spectrum (Figure 5a,b). Thus, both $[WO_6]$ and $[AgO_x]$ distorted clusters, which represent the network former and modifier, respectively, act together to produce a large amount of ·OH* and ·O_2H^*. Hence, the α-Ag_2WO_4 microcrystals synthesized using the alcoholic solution exhibit a better antimicrobial efficiency compared to the other microcrystals (Figure 10).

In addition, Roca et al.[39] have observed that the (010) face of the α-Ag_2WO_4 crystals exhibits low surface energy (0.20 J/m^2), as determined by ab initio calculations, and it is more efficient for the inactivation of bacteria compared to the other faces.[39] As previously observed in the FE-SEM images (Figure 3A−C),

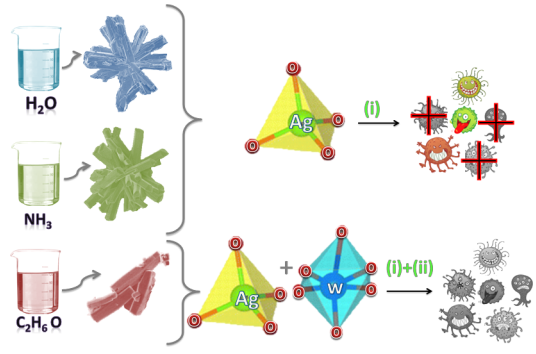

Figure 10. Proposed action mechanism for the antimicrobial effect of the catalysts α-Ag_2WO_4 microcrystals.

DOI: 10.1021/acs.cgd.7b00786
Cryst. Growth Des. 2017, 17, 6239−6246

the α-Ag_2WO_4 synthesized using the alcoholic solution exhibits a larger amount of the (010) face compared with that synthesized using the ammoniacal solution and water. As the formation of flowers decreases the amount of the exposed (010) face, the α-Ag_2WO_4 microcrystals synthesized using alcohol showed the higher activity against all tested microorganisms, in comparison to the other solvents.

Based on the molecular weight of each component, the actual silver content of the α-Ag_2WO_4 microcrystals at the MFC/MBC concentrations was calculated. For *C. albicans*, the content of silver in α-Ag_2WO_4 synthesized using the alcoholic solution is 0.0018 μg/mL, and that in α-Ag_2WO_4 synthesized using water and the ammoniacal solution is 0.0036 μg/mL. For MRSA, the content of silver in the microcrystals synthesized using the alcoholic solution, ammoniacal solution, and water is 0.0072, 0.029, and 0.057 μg/mL, respectively. With regard to *E. coli*, the α-Ag_2WO_4 microcrystals synthesized using the alcoholic and ammoniacal solutions exhibit the same silver content (0.00023 μg/mL). This value is less than that observed using water as the solvent (0.00045 μg/mL). The content of silver in all of the synthesized α-Ag_2WO_4 microcrystals is extremely low. In addition, as mentioned before, the alcoholic solution produces α-Ag_2WO_4 microcrystals with a stronger antifungal/antibacterial activity, thereby considerably decreasing the concentrations required to kill the three microorganisms; hence, the amount of silver used decreases.

5. CONCLUSIONS

With the progress in materials science research, different semiconductor materials corresponding to complex metal oxides demonstrate potential as potent antimicrobial agents. Here, α-Ag_2WO_4 microcrystals are obtained by coprecipitation using different solvents. These microcrystal structures are characterized by XRD, Raman spectroscopy, and FE-SEM, while their optical properties are studied by UV−vis diffuse reflectance spectroscopy and PL measurements. Our studies demonstrated that α-Ag_2WO_4 microcrystals exhibit antibacterial activity against the planktonic cells of the yeast *C. albicans*, the Gram-positive bacterium MRSA, and the Gram-negative bacterium *E. coli*.

On the basis of these results, α-Ag_2WO_4 microcrystals are introduced as a new family of antimicrobial materials for their potential use in water treatment and biomedical applications. Hence, this investigation is useful for authenticating the α-Ag_2WO_4 microcrystals as an antibacterial agent. Besides that, this research provides helpful insight into the development of novel antibacterial agents. Currently, more detailed experiments to explain the nature of the corresponding mechanism of antibacterial activity are underway in our laboratory.

AUTHOR INFORMATION

Corresponding Author

*E-mail: camilafoggi@yahoo.com.br.

ORCID

Camila C. de Foggi: 0000-0002-1210-1234
Regiane C. de Oliveira: 0000-0002-7332-8731
Juan Andres: 0000-0003-0232-3957

Notes

The authors declare no competing financial interest.

ACKNOWLEDGMENTS

The authors are grateful to FAPESP (FAPESP-CDMF: 2013/07296-2 and FAPESP 2015/03654-7), CNPq (304190/2013-6), and CAPES (for financial support of this research). J.A. acknowledges the following Spanish research funding institutions: *PrometeoII*/2014/022 and ACOMP/2015/1202 projects (Generalitat-Valenciana), Ministerio de Economia y Competitividad (CTQ2015-65207-P), Programa de Cooperación Científica. con Iberoamerica (Brasil) of Ministerio de Educación (PHBP14-00020), and Ministerio de Economia y Competitividad, "Salvador Madariaga" program, PRX15/00261.

REFERENCES

(1) Dai, X.-J.; Luo, Y.-S.; Zhang, W.-D.; Fu, S.-Y. *Dalton Trans.* **2010**, *39* (14), 3426−3432.
(2) Muthamizh, S.; Suresh, R.; Giribabu, K.; Manigandan, R.; Kumar, S. P.; Munusamy, S.; Narayanan, V. *J. Alloys Compd.* **2015**, *619*, 601−609.
(3) Zhang, G.; Yang, S.; Li, Z.; Zhang, L.; Zhou, W.; Zhang, H.; Shen, H.; Wang, Y. *Appl. Surf. Sci.* **2010**, *257* (1), 302−305.
(4) Rajagopal, S.; Nataraj, D.; Khyzhun, O. Y.; Djaoued, Y.; Robichaud, J.; Mangalaraj, D. *J. Alloys Compd.* **2010**, *493* (1), 340−345.
(5) Lin, C.; Jiexin, C.; Cong, W.; Ping, C.; DE'AN, P.; Volinsky, A. A. *Bull. Mater. Sci.* **2012**, *35* (5), 767−772.
(6) Boulon, G. *Opt. Mater.* **2012**, *34* (3), 499−512.
(7) Xu, D.; Cheng, B.; Zhang, J.; Wang, W.; Yu, J.; Ho, W. *J. Mater. Chem. A* **2015**, *3* (40), 20153−20166.
(8) Zhang, Z.; Wang, W.; Jiang, D.; Xu, J. *Appl. Surf. Sci.* **2014**, *292*, 948−953.
(9) De Santana, Y. V.; Gomes, J. E. C.; Matos, L.; Cruvinel, G. H.; Perrin, A.; Perrin, C.; Andrès, J.; Varela, J. A.; Longo, E. *Nanomater. Nanotechnol.* **2014**, *4*, 22.
(10) Song, Q.-W.; Yu, B.; Li, X.-D.; Ma, R.; Diao, Z.-F.; Li, R.-G.; Li, W.; He, L.-N. *Green Chem.* **2014**, *16*, 1633−1638.
(11) Guo, C.-X.; Yu, B.; Xie, J.-N.; He, L.-N. *Green Chem.* **2015**, *17*, 474−479.
(12) Longo, V. M.; De Foggi, C. C.; Ferrer, M. M.; Gouveia, A. F.; André, R. S.; Avansi, W.; Vergani, C. E.; Machado, A. L.; Andrés, J.; Cavalcante, L. S.; Hernandes, A. C.; Longo, E. *J. Phys. Chem. A* **2014**, *118* (31), 5769−5778.
(13) Cheng, L.; Shao, Q.; Shao, M.; Wei, X.; Wu, Z. *J. Phys. Chem. C* **2009**, *113* (5), 1764−1768.
(14) Cavalcante, L. S.; Almeida, M. A. P.; Avansi, W.; Tranquilin, R. L.; Longo, E.; Batista, N. C.; Mastelaro, V. R.; Li, M. S. *Inorg. Chem.* **2012**, *51* (20), 10675−10687.
(15) Zhang, R.; Cui, H.; Yang, X.; Tang, H.; Liu, H.; Li, Y. *Micro Nano Lett.* **2012**, *7* (12), 1285−1288.
(16) Liu, X.; Hu, J.; Li, J.; Hu, Y.; Shao, Y.; Yang, H.; Tong, G.; Qian, H. *Mater. Lett.* **2013**, *91*, 129−132.
(17) Chen, H.; Xu, Y. *Appl. Surf. Sci.* **2014**, *319*, 319−323.
(18) Tang, J.; Ye, J. *J. Mater. Chem.* **2005**, *15* (39), 4246−4251.
(19) Wang, X.; Fu, C.; Wang, P.; Yu, H.; Yu, J. *Nanotechnology* **2013**, *24* (16), 165602.
(20) Stone, D.; Liu, J.; Singh, D. P.; Muratore, C.; Voevodin, A. A.; Mishra, S.; Rebholz, C.; Ge, Q.; Aouadi, S. M. *Scr. Mater.* **2010**, *62* (10), 735−738.
(21) Pan, L.; Li, L.; Chen, Y. *J. Sol-Gel Sci. Technol.* **2013**, *66* (2), 330−336.
(22) da Silva, L. F.; Catto, A. C.; Avansi, W.; Cavalcante, L. S.; Andrés, J.; Aguir, K.; Mastelaro, V. R.; Longo, E. *Nanoscale* **2014**, *6*, 4058−4062.
(23) Wang, Q. P.; Guo, X. X.; Wu, W. H.; Liu, S. X. *Adv. Mater. Res.* **2011**, *284−286*, 1321−1325.
(24) Longo, E.; Cavalcante, L. S.; Volanti, D. P.; Gouveia, A. F.; Longo, V. M.; Varela, J. A.; Orlandi, M. O.; Andrés, J. *Sci. Rep.* **2013**, *3*, 1676.

DOI: 10.1021/acs.cgd.7b00786
Cryst. Growth Des. 2017, 17, 6239−6246

(25) Longo, E.; Volanti, D. P.; Longo, V. M.; Gracia, L.; Nogueira, I. C.; Almeida, M. A. P.; Pinheiro, A. N.; Ferrer, M. M.; Cavalcante, L. S.; Andrés, J. *J. Phys. Chem. C* **2014**, *118* (2), 1229−1239.
(26) Andrés, J.; Gracia, L.; Gonzalez-Navarrete, P.; Longo, V. M.; Avansi, W.; Volanti, D. P.; Ferrer, M. M.; Lemos, P. S.; La Porta, F. A.; Hernandes, A. C.; Longo, E. *Sci. Rep.* **2015**, *4*, 5391.
(27) Pereira, W. d. S.; Andrés, J.; Gracia, L.; San-Miguel, M. A.; da Silva, E. Z.; Longo, E.; Longo, V. M. *Phys. Chem. Chem. Phys.* **2015**, *17* (7), 5352−5359.
(28) Zhang, X.-Y.; Wang, J.-D.; Liu, J.-K.; Yang, X.-H.; Lu, Y. *CrystEngComm* **2015**, *17* (5), 1129−1138.
(29) da Silva, L. F.; Catto, A. C.; Avansi, W.; Cavalcante, L. S.; Mastelaro, V. R.; Andrés, J.; Aguir, K.; Longo, E. *J. Alloys Compd.* **2016**, *683*, 186−190.
(30) Hu, B.; Wu, L.-H.; Zhao, Z.; Zhang, M.; Chen, S.-F.; Liu, S.-J.; Shi, H.-Y.; Ding, Z.-J.; Yu, S.-H. *Nano Res.* **2010**, *3* (6), 395−403.
(31) Wang, Q. P.; Guo, X. X.; Wu, W. H.; Liu, S. X. *Adv. Mater. Res.* **2011**, *284*, 1321−1325.
(32) Wojcieszak, D.; Mazur, M.; Kaczmarek, D.; Szponar, B.; Grobelny, M.; Kalisz, M.; Pelczarska, A.; Szczygiel, I.; Poniedzialek, A.; Osekowska, M. *Appl. Surf. Sci.* **2016**, *380*, 159−164.
(33) Lee, S. J.; Heo, D. N.; Moon, J.-H.; Ko, W.-K.; Lee, J. B.; Bae, M. S.; Park, S. W.; Kim, J. E.; Lee, D. H.; Kim, E.-C. *Carbohydr. Polym.* **2014**, *111*, 530−537.
(34) Nanda, S. S.; Yi, D. K.; Kim, K. *Sci. Rep.* **2016**, *6*, 28433.
(35) Tang, Z.-X.; Fang, X.-J.; Zhang, Z.-L.; Zhou, T.; Zhang, X.-Y.; Shi, L.-E. *Braz. J. Chem. Eng.* **2012**, *29* (4), 775−781.
(36) Tang, Z.-X.; Lv, B.-F. *Braz. J. Chem. Eng.* **2014**, *31* (3), 591−601.
(37) Barbolina, I.; Woods, C.; Lozano, N.; Kostarelos, K.; Novoselov, K.; Roberts, I. *2D Mater.* **2016**, *3* (2), 025025.
(38) Buccheri, M. A.; D'Angelo, D.; Scalese, S.; Spanò, S. F.; Filice, S.; Fazio, E.; Compagnini, G.; Zimbone, M.; Brundo, M. V.; Pecoraro, R.; et al. *Nanotechnology* **2016**, *27* (24), 245704.
(39) Roca, R. A.; Sczancoski, J. C.; Nogueira, I. C.; Fabbro, M. T.; Alves, H. C.; Gracia, L.; Santos, L. P. S.; de Sousa, C. P.; Andres, J.; Luz, G. E.; Longo, E.; Cavalcante, L. S. *Catal. Sci. Technol.* **2015**, *5* (8), 4091−4107.
(40) Fabbro, M. T.; Foggi, C. C.; Santos, L. P.; Gracia, L.; Perrin, A.; Perrin, C.; Vergani, C. E.; Machado, A. L.; Andrés, J.; Cordoncillo, E.; et al. *Dalton Trans.* **2016**, *45* (26), 10736−10743.
(41) Clinical and Laboratory Standards Institute. *Reference Method for Broth Dilution Antifungal Susceptibility Testing of Yeasts*; CLSI Document M27-A3; Clinical and Laboratory Standards Institute: Wayne, PA, 2008.
(42) Clinical and Laboratory Standards Institute. *Methods for Dilution Antimicrobial Susceptibility Tests for Bacteria That Grow Aerobically*; CLSI Document M7-A7; Clinical and Laboratory Standards Institute: Wayne, PA, 2006
(43) Zamperini, C. A.; André, R. S.; Longo, V. M.; Mima, E. G.; Vergani, C. E.; Machado, A. L.; Varela, J. A.; Longo, E. *J. Nanomater.* **2013**, *2013*, 174398.
(44) André, R. S.; Zamperini, C. A.; Mima, E. G.; Longo, V. M.; Albuquerque, A. R.; Sambrano, J. R.; Machado, A. L.; Vergani, C. E.; Hernandes, A. C.; Varela, J. A.; Longo, E. Antimicrobial activity of TiO2:Ag nanocrystalline heterostructures: Experimental and theoretical insights. *Chem. Phys.* **2015**, *459*, 87−95.
(45) Skarstad, P. M.; Geller, S. *Mater. Res. Bull.* **1975**, *10* (8), 791−799.
(46) Lin, Z.; Li, J.; Zheng, Z.; Yan, J.; Liu, P.; Wang, C.; Yang, G. *ACS Nano* **2015**, *9* (7), 7256−7265.
(47) Yan, T.; Li, L.; Tong, W.; Zheng, J.; Wang, Y.; Li, G. *J. Solid State Chem.* **2011**, *184* (2), 357−364.
(48) Kubelka, P.; Munk, F. *Z. Tech Phys.* **1931**, *12*, 593−601.
(49) Kim, D. W.; Cho, I.-S.; Lee, S.; Bae, S.-T.; Shin, S. S.; Han, G. S.; Jung, H. S.; Hong, K. S. *J. Am. Ceram. Soc.* **2010**, *93* (11), 3867−3872.
(50) Longo, V. M.; Cavalcante, L. S.; Paris, E. C.; Sczancoski, J. C.; Pizani, P. S.; Li, M. S.; Andrés, J.; Longo, E.; Varela, J. A. *J. Phys. Chem. C* **2011**, *115* (13), 5207−5219.
(51) *PeakFit*, version 4.12; Systat Software, Inc.: San Jose, CA.
(52) Gong, Q.; Qian, X.; Ma, X.; Zhu, Z. *Cryst. Growth Des.* **2006**, *6* (8), 1821−1825.
(53) Chen, D.; Tang, K.; Li, F.; Zheng, H. *Cryst. Growth Des.* **2006**, *6* (1), 247−252.
(54) Longo, V.; Cavalcante, L. d.; De Figueiredo, A.; Santos, L.; Longo, E.; Varela, J. A.; Sambrano, J.; Paskocimas, C.; De Vicente, F.; Hernandes, A. *Appl. Phys. Lett.* **2007**, *90*, 091906.
(55) Wyckoff, R. W. G. *Crystal Structures*; Wiley: New York, 1948; Vol. *II*.
(56) Phuruangrat, A.; Thongtem, T.; Thongtem, S. *J. Cryst. Growth* **2009**, *311* (16), 4076−4081.
(57) Phuruangrat, A.; Thongtem, T.; Thongtem, S. *J. Phys. Chem. Solids* **2009**, *70* (6), 955−959.
(58) Longo, V. M.; Picon, F. C.; Zamperini, C.; Albuquerque, A. R.; Sambrano, J. R.; Vergani, C. E.; Machado, A. L.; Andrés, J.; Hernandes, A. C.; Varela, J. A.; et al. *Chem. Phys. Lett.* **2013**, *577*, 114−120.
(59) Zhao, G.; Stevens, S. E., Jr *BioMetals* **1998**, *11* (1), 27−32.
(60) Ninganagouda, S.; Rathod, V.; Singh, D.; Hiremath, J.; Singh, A. K.; Mathew, J.; ul-Haq, M. *BioMed Res. Int.* **2014**, *2014*, 753419.
(61) Yamanaka, M.; Hara, K.; Kudo, J. *Appl. Environ. Microbiol.* **2005**, *71*, 7589−7593.
(62) Xu, J.-W.; Gao, Z.-D.; Han, K.; Liu, Y.; Song, Y.-Y. *ACS Appl. Mater. Interfaces* **2014**, *6* (17), 15122−15131.

DOI: 10.1021/acs.cgd.7b00786
Cryst. Growth Des. 2017, 17, 6239−6246